PCCP

ROYAL SOCIETY OF CHEMISTRY

PAPER

View Article Online
View Journal | View Issue

Cite this: *Phys. Chem. Chem. Phys.*, 2024, **26**, 517

Exploring fullerene derivatives for optoelectronic applications: synthesis and characterization study†

Jovana Jakšić,[a] Evgenija Milinković,[b] Katarina Cvetanović,[b] Zorana Tokić Vujošević,[c] Vladislav Jovanov,[b] Aleksandra Mitrović *[a] and Veselin Maslak *[a]

Received 6th September 2023,
Accepted 1st December 2023

DOI: 10.1039/d3cp04322c

rsc.li/pccp

In this study, we conducted a comprehensive investigation of newly synthesized fullerene derivatives developed for potential application in perovskite solar cells (PSCs). We explored three novel dihydrofuran-fused C_{60} fullerene derivatives (**13**, **14**, and **15**) that were specifically designed to enhance solubility and interaction with the substrate, fluorine-doped tin oxide (**FTO**). A comparative analysis was performed, with reference to the widely used phenyl-C61-butyric acid methyl ester (PCBM) and compound **12**, from which **13**, **14**, and **15** are derived, to assess the impact of sugar units on materials properties. The synthesized compounds demonstrated significant solubility in common organic solvents, a critical factor in their potential application in wet-processed PSCs. Our investigation included electrochemical property analysis, thin film deposition, surface characterization, and electrochemical impedance spectroscopy (EIS). EIS measurements unveiled key insights into charge transfer properties at the electrode/electrolyte interface, making the compounds attractive candidates for electron transport layers (ETLs) in PSCs.

Introduction

In the last decade, metal halide perovskite materials have garnered significant scientific interest, resulting in numerous studies exploring their physical properties and their incorporation in various optoelectronic devices such as solar cells, photodetectors (including X-ray detectors), light-emitting diodes, and lasers.[1–4] Significant progress has been made in comprehending the fundamental crystallographic, optical, and electrical properties of perovskite materials. These advancements have led to a substantial increase in the power conversion efficiency of perovskite solar cells, rising from 3.8% to 25.7% in a decade, surpassing the efficiency of silicon-based multicrystalline solar cells (22.3%), copper indium gallium selenide (23.4%), and cadmium telluride (CdTe, 22.1%).[5–12] Perovskite-based solar cells have numerous fabrication advantages since they can be easily deposited on lightweight, flexible plastic foils.

In a perovskite solar cell, ETL plays a crucial role in facilitating the movement of electrons from the perovskite layer to the anode contact.[13] Traditionally, these materials have faced limitations, primarily stemming from issues of stability, performance, and fabrication compatibility. Among the contenders, titanium dioxide (TiO_2) has held a prominent position due to its electron transport capabilities; however, it has been marred by challenges linked to high-temperature processing and potential electrical instabilities.[14] Amidst these challenges, a remarkable contender has risen to prominence – fullerenes, particularly fullerene derivatives, which have exhibited a level of resilience and enduring performance that justifies their characterization as "immortal" within the realm of PSCs.[15]

Advancement in fullerene chemistry[16] and the synthesis of various solution-processable derivatives have propelled their widespread adoption as key components in various electronic devices. Notably, the phenyl-C61-butyric acid methyl ester (PCBM)[17] is employed in a variety of applications, including organic solar cells[18–21] and perovskite or inverted perovskite solar cells.[22–25]

When applied as ETLs in inverted perovskite solar cells, fullerene derivatives offer numerous advantages. These include improved electron transport, seamless compatibility with perovskite materials, and reduced hysteresis effects.[26,27] To address limitations encountered with PCBM, such as limited solubility in aromatic solvents, sensitivity to light-soaking effects, and moisture susceptibility, diverse structural

[a] *Faculty of Chemistry, University of Belgrade, Studenstki trg 12, 11158, Belgrade, Serbia*
[b] *Institute of Chemistry, Technology and Metallurgy, University of Belgrade, Njegoševa 12, 11000 Belgrade, Serbia*
[c] *Department of Organic Chemistry, University of Belgrade, Faculty of Pharmacy, Vojvode Stepe 450, 11221 Belgrade, Serbia*

† Electronic supplementary information (ESI) available. See DOI: https://doi.org/10.1039/d3cp04322c

modifications have been explored, with successful derivatives featuring heterocyclic compounds containing nitrogen (N) and oxygen (O) atoms in ester or ether groups[28–32]

In this context, we have utilized cost-effective nitro-substituted sugars, specifically isosorbide, and isomanide, as starting materials to synthesize well-suited C_{60} derivatives. The development of novel fullerene derivatives holds immense promise for enhancing the efficiency and stability of perovskite solar cells, although it remains a challenging endeavor.[23,33] Furthermore, conducting exhaustive characterization for individual perovskite solar cells corresponding to each compound within the series entails significant labour and resources. Recognizing this challenge, our research aimed to streamline the procedure by implementing a more efficient approach that eliminates the need for building complete solar cells. This approach allowed us to evaluate compounds based on essential characteristics such as absorption and charge transport properties. Consequently, it expedited the assessment of their potential, providing valuable insights into their suitability for perovskite solar cells.

In this study, we synthesized three novel fullerene derivatives, differing solely in their stereochemistry. This methodology was developed to effectively distinguish and discern between these compounds, facilitating a more efficient evaluation process.

Results and discussion

The dihydrofuran-fused C_{60} fullerene derivatives with sugar units (**13**, **14**, **15**) were synthesized following the procedure outlined in Scheme 1. The incorporation of sugar units was intended to enhance solubility and explore their interaction with the substrate, which is fluorine-doped tin oxide (FTO).

For comparison, we selected **PCBM** as a well-known material and compound **12** as the reference material (as shown in Scheme 1). Compound **12**, dihydrofuran C_{60} with an ethyl group, which had been synthesized previously,[34] was chosen to assess whether the addition of a sugar component affects the material's properties. The fullerene-sugar adducts **13**, **14**, and **15** were obtained in a multistep synthetic route in which pristine fullerene C_{60} was covalently connected to the sugar by oxidative cycloaddition, which involved the preparation of the corresponding β-keto ester-sugar derivates as shown in Scheme 1.

The starting material, 3-oxooctanoic acid **2**, was obtained with an 81% yield through the hydrolysis of methyl 3-oxooctanoate derived from Meldrum acid and hexanoyl chloride (as described in the ESI†). Despite the β-keto ester's propensity for decarboxylation, we successfully obtained the desired 3-oxooctanoic acid **2** in a good yield. The coupling of 3-oxooctanoic acid **2** with different isohexides (1,4:3,6-dianhydrohexitols) mononitrates was carried out using *N*,*N*′-dicyclhexylcarbodiimide (DCC) and 4-dimethylaminopyridine (DMAP) in dichloromethane (DCM) at room temperature for 24 hours, resulting in a 68–70% yield for sugar derivatives **6**, **8**, and **10**. We used the commercially available isosorbide 5-mononitrate **5**, isosorbide 2-mononitrate **7**, while isomannide 5-mononitrate **9** was synthesized from neat isomannide through a sequence of reactions (as described in the ESI†). β-Keto esters possess an ambivalent nature due to the presence of both a carbonyl group and an α-hydrogen atom. This property renders them highly reactive towards a variety of nucleophiles and electrophiles, making them useful intermediates in many organic transformations. In a recent paper, we presented the synthesis of furan-fused fullerenes using a simple reaction protocol for oxidative

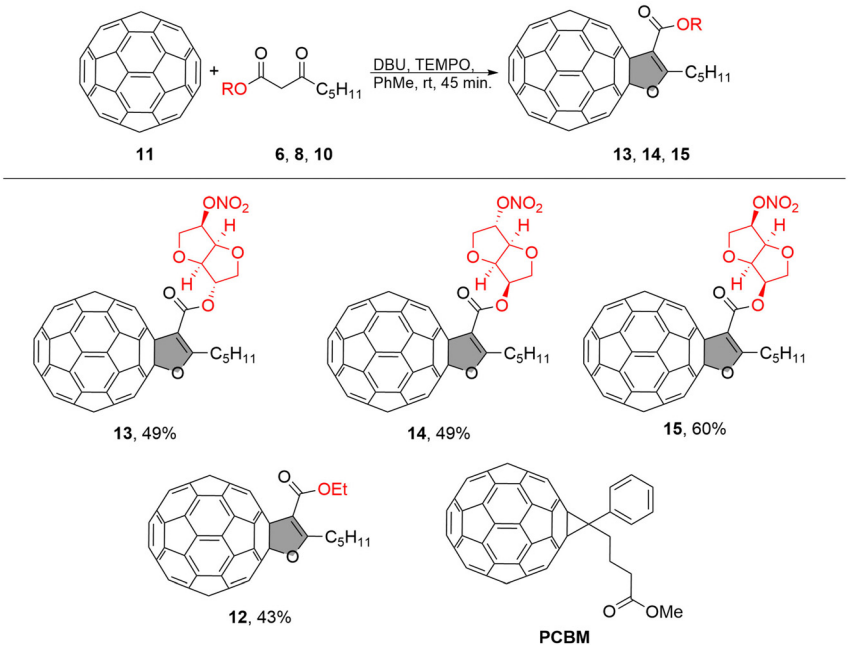

Scheme 1 Synthetic protocol for obtaining fullerene derivatives **13**, **14**, **15** and their structures along with the reference compounds **12** and **PCBM**.

cycloaddition reaction between medium chain β-keto esters and **C_{60}** in the presence of DBU and 2,2,6,6-tetramethylpiperidine-1-oxy (TEMPO) in toluene for 45 minutes at room temperature.[34,35] The resulting procedure was now used to synthesize fullerene-sugar adducts **13**, **14**, and **15**, which were obtained in yields ranging from 49% to 60%.

Dihydrofuran-fused fullerenes **13**, **14**, and **15** were synthesized for the first time with very good yields. Their structures were confirmed using HRMS, ^{1}H NMR, ^{13}C NMR, and UV-Vis (see ESI†). These products showed significant solubility in common organic solvents such as toluene, dichloromethane, and chloroform (approx. 40–60 mg mL^{-1}). Due to the challenges in precisely estimating the solubility of intensely coloured compounds, the solubility of **14** was assessed using UV-Vis spectroscopy as a representative of the other compounds since they only differ in the stereochemistry of the sugar addend.[35] The results indicated that **14** is soluble in toluene at concentrations of 60 mg mL^{-1}. The significance of this property of furan-fused fullerenes lies in their potential applications and their amenability to processing in material chemistry. This is particularly noteworthy when considering that the solubility of **PCBM** in toluene does not surpass 19 mg mL^{-1}.[36]

The electrochemical properties of **C_{60}**, **PCBM**, and dihydrofuran-fused fullerenes **12**, **13**, **14**, and **15** were investigated through cyclic voltammetry and linear sweep voltammetry (LSV) in solution. The resulting cyclic voltammetry (CV) and linear sweep voltammetry (LSV) data have been compiled in Table 1.

The obtained products **12**, **13**, **14**, and **15** exhibited four reversible reduction waves, which were attributed to the successive reductions of the **C_{60}** cage (refer to Fig. S41–S46, ESI†). The first reduction potentials (E^1_{red}) of the reaction products were similar to those of **C_{60}**. Generally, when the C_{2v} symmetry of **C_{60}** is disrupted, it becomes more challenging for the derivative to accept an electron. In this particular case, the dihydrofuran-fused fullerenes displayed either similar or slightly more negative values for the first reduction, consistent with the established rule.

Furthermore, we utilized the potential at the first reduction peak (E^1_{red}) to calculate the LUMO energy levels relative to the standard potential of the reference electrode. This calculation was performed using the following equation: E(LUMO) = $-(E^1_{red} + 4.8)$ (eV). The energy gap for each compound was determined through Tauc plot analysis of the UV-Vis spectra in toluene.[37–39] Subsequently, the final HOMO energy levels for each compound were calculated using the equation: E(HOMO) = E(LUMO) − energy gap (eV) (refer to Table 1 for details). The calculated energy levels are slightly higher than those of **PCBM**, as are the values of E_g.

To assess the quality of the thin films generated by our compounds, they were deposited onto glass substrates. The samples, which were spin-coated in a consistent manner, displayed comparable absorbance intensity, which could be attributed to the uniform thickness achieved through the specified spin-coating parameters (see Fig. S48, ESI†). After the layers were washed from the plates, it was observed that the quantities of the samples exhibited minimal variation within the range of 0.3 mg to 0.5 mg. When these thin films were examined under AFM, several characteristics were detected (as depicted in Fig. 1 and Fig. S60–S64 in the ESI†). Reference compound **12**, lacking a sugar moiety, formed spherical assemblies with distinct, round repetitive features (see Fig. S60, ESI†). Conversely, **PCBM** and the fullerene derivatives **13–15** exhibited relatively smooth surfaces, indicating the absence of significant aggregates on a molecular scale. The reduced roughness on the surface of the ETL can lead to a smoother interface between the ETL and the active layer.

Following the initial characterization of the thin films, further investigation of the fullerene derivatives involved their deposition onto the **FTO** substrate. The significant surface roughness of **FTO** posed a challenge in detecting the molecular arrangements of the samples (see Fig. S65–S66, ESI†). With the Raman spectroscopy (Fig. 2) we were able to see that, unlike glass, **FTO** does not provide complete coverage. Instead, the signals associated with fullerenes were detected mostly within the valleys of the wave-like **FTO** pattern.

Considering the non-homogeneous nature of the surface on a microscopic scale, we conducted electrochemical impedance spectroscopy (EIS) measurements. These measurements involved the bare **FTO** sample as well as the fullerene samples

Table 1 Half-wave reduction potentials (V *vs.* Fc/Fc+) of **C_{60}**, **PCBM**, and furan-fused fullerenes **12**, **13**, **14**, **15** in solution. λ_{abs} represents the absorption peaks used in Tauc plot analysis

Compd	E^1_{red} (V)	LUMO (eV)	E_g (eV)	HOMO (eV)	λ_{abs} (nm)
C_{60}	−1.14	−3.66	1.70	−5.36	729
12	−1.16	−3.64	1.76	−5.40	704
13	−1.12	−3.68	1.75	−5.43	708
14	−1.15	−3.65	1.77	−5.42	700
15	−1.14	−3.66	1.77	−5.43	700
PCBM	−1.24	−3.56	1.73	−5.29	717

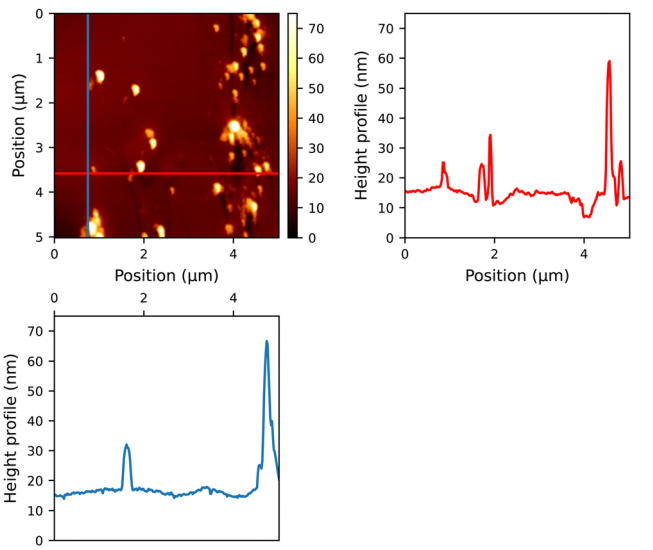

Fig. 1 AFM of the sample **15** on the glass substrate.

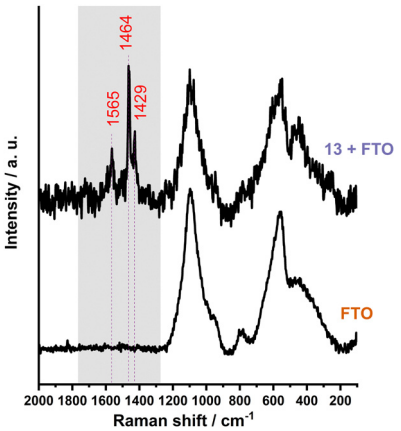

Fig. 2 The Raman spectrum (λ_{max} = 532 nm) of the sample **13** displays bands corresponding to C–C (1429 cm^{-1}), C=C (1464 cm^{-1}) and C=O (1565 cm^{-1}) vibrations.

deposited on **FTO** and were analyzed using an equivalent circuit.[40] (see Fig. 3).

Elements of the equivalent circuits are R_s – resistance of wiring; R_{ct} – resistance of charge transfer at the solid–electrolyte interface (double layer interface); Q_{dl} – also noted as CPE (constant phase element), which represents the component that models the capacitive behavior of the working electrodes, which can be explained as an imperfect capacitor. Its impedance can be expressed as:

$$Z_{CPE} = (j\omega)^{-n}C^{-1}$$

where C is the capacitance of an ideal capacitor, ω is the angular frequency, j is the complex number, and n is a parameter ranging from 0 to 1, depending on the electrode's nature. Value n = 0 denotes the CPE of a resistor, and n = 1 denotes the CPE is the ideal capacitor. In Fig. 3, the components R_{ct} and Q_{dl} address the charge transfer at the working electrode/electrolyte interface, while W addresses the diffusion of the electroactive component in the electrolyte, namely $Fe^{3+/4+}(CN)_6$ redox couple. Meanwhile, R_s represents the resistance of all other circuit components combined, including the resistance of the cables. Fitting results are presented in Table 2.

The R_s (solution resistance) value was found to be similar for all samples, mainly determined by the experimental setup and conditions. The Nyquist diagrams revealed a semi-circle

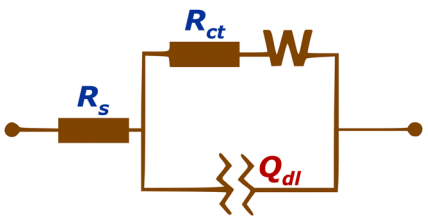

Fig. 3 Equivalent circuits used for fitting: R_s – resistance of the wiring, R_{ct} – resistance of charge transfer at the solid-electrolyte interface (double layer interface); Q_{dl} – CPE (constant phase element), W – Warburg impedance, representing the diffusion process in the vicinity of the electrode.

Table 2 Parameters values obtained from the EIS data fitting

Sample	R_s (Ω)	R_{ct} (Ω)	W $s^{(1/2)}/\Omega$	Q_{dl} $(s^N/\Omega) \times 10^{-6}$	n
FTO	21.2	41.0	0.028	4.60	0.942
12	24.7	19.1	0.007	9.97	1.000
13	49.9	34.1	0.020	7.95	0.996
14	48.7	35.9	0.025	4.62	1.000
15	27.1	36.7	0.024	6.36	1.000
PCBM	32.9	42.4	0.021	9.87	0.922

representing the charge-transfer process at the interface for all samples (Fig. 4).

From the results in Table 2, samples **13**, **14**, and **15**, which contain sugar units, exhibited comparable charge transfer resistance values at the electrode/electrolyte interface (34.1, 35.9, and 36.7 Ω). These values were lower than those observed for the bare **FTO** and **PCBM** samples (41.0 and 42.4 Ω), indicating facilitated charge transfer on surfaces with sugar units. Notably, the furan-fused fullerene derivative, sample **12**, had the smallest R_{ct} value of 19.1 Ω, suggesting its potential as an ETL candidate.

EIS measurements also revealed a diffusion process indicated by a 45° line in the Nyquist diagram for all samples (Fig. 4). This process results from fast charge transfer and the creation of a depletion region near the electrode surface, driven by a concentration gradient of the $Fe^{3+/4+}(CN)_6$ redox couple. All samples showed similar values of the Warburg impedance, indicating consistent behaviour of electroactive species in the electrolyte. The smallest Warburg impedance was observed for sample **12**.

The Q_{dl} values, representing the diameter of the charge-transfer semi-circle, suggest that the amount of deposited material may vary but is of the same order of magnitude for all samples. The n value was close to 1 for samples **12**, **13**, **14**, and **15**, suggesting the nature of the ideal capacitor.

Bode diagrams for the measured samples are presented in Fig. S65 (ESI†). The peak position in the Bode phase diagram is used for the determination of the electron lifetime (τ) in the

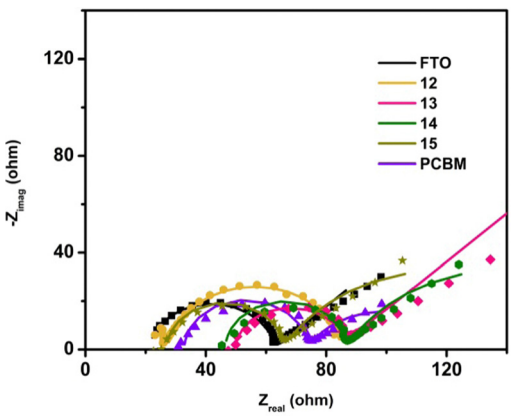

Fig. 4 Nyquist diagram obtained by fitting the experimental result with the equivalent circuit from Fig. 1. Symbols represent experimental data, while straight lines represent the results of the fitting with an equivalent circuit.

Table 3 Electron lifetime in the samples

Sample	FTO	12	13	14	15	PCBM
T (ms)	0.06	0.54	0.21	0.20	0.18	0.28

Table 4 Peak-to-peak value of the measured samples

Sample	FTO	12	13	14	15	PCBM
ΔU_{p-p}(V)	0.409	0.216	0.397	0.380	0.379	0.448

samples ($\tau = 1/2\pi f_{max}$), where f_{max} is the corresponding frequency of the peak maximum.[41] Obtained values are presented in Table 3. The electron lifetime of samples **13**, **14**, and **15** are once again similar, while sample **12** has a significantly higher value of this parameter, indicating that this sample has a slower rate of charge carrier recombination. In the impedance magnitude diagram, one can notice a small shift of the peak toward lower frequencies, for samples **13**, **14**, **15**, and especially sample **12**, compared to **FTO**. This shift can also indicate the faster charge transfer in these samples.

Additional information on the conductivity of the films was provided by studying the cyclic voltammetry response of a molecular probe on the film-coated electrode (Fig. 5). In this experiment, potassium ferro/ferricyanide was used as the molecular probe because it undergoes a reversible, one-electron redox reaction. Measured voltammograms are presented in Fig. 5, top. For the quantification of the conductivity, peak-to-peak distance was determined for each sample. The obtained results are presented in Table 4, an example of the peak-to-peak determination is given in Fig. 5, bottom. The smallest value of the calculated parameter is obtained for sample **12**, meaning that this sample has the highest responsivity among all samples, 0.216 V, compared to the value obtained for the **FTO** of 0.403 V. Also, samples **13**, **14**, and **15** had somewhat smaller values for U_{p-p} of 0.397, 0.380, and 0.379 V.

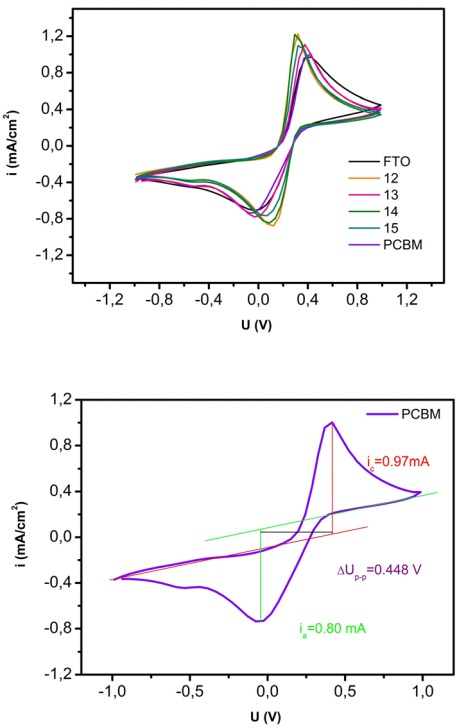

Fig. 5 (top) Cyclic voltammograms of the measured samples **12**, **13**, **14**, **15** and **PCBM** on **FTO**, (bottom) Measurement of the peak-to-peak potential for the **PCBM** sample.

Conclusions

We synthesized three new fullerene derivatives and conducted a comprehensive characterization study to explore their potential for optoelectronic applications. The synthesized dihydrofuran-fused C_{60} fullerene derivatives with sugar units (compounds **13**, **14**, and **15**) exhibited significant solubility in common organic solvents, which is crucial for their possible application in material chemistry. Considering the successful use of fullerenes in ETLs by T. Kirchartz's group, featuring a bandgap of $E_g = 1.72$ eV, resulting in open-circuit voltages exceeding 1.35 V and a power conversion efficiency enhancement of up to 18.9%, our samples, with a similar bandgap of around 1.7 eV, present promising candidates for solar cell construction.[42]

Samples **13**, **14**, and **15**, with particular emphasis on sample **12**, exhibited lower values for charge transfer resistance and peak-to-peak potential compared to the reference **PCBM**. This suggests their potential to enhance charge transfer properties in perovskite solar cells. Additionally, AFM analysis revealed low roughness on flat surfaces, which could prove beneficial for an ETL. These results open up new avenues for further research and the optimization of these derivatives, contributing to the advancement of renewable energy technologies.

Materials and methods

Fullerene **C_{60}** and **PCBM** were bought from Merck.

Sample preparation for spin-coating followed a standardized procedure. All substrates underwent the same cleaning process, involving ultrasonic treatment in detergent for 15 minutes, rinsing with DI water, and drying with N_2. This was followed by ultrasonic treatment in isopropanol for 2 minutes, drying with N_2, and immersing in acetone for 2 minutes, followed by N_2 drying. After ultrasonic treatments, substrates were rinsed with ethanol, dried with N_2, and exposed to an 18 minute UV-ozone cleaner treatment as a final step. In this study, the spin-coating method was employed for deposition. The toluene solution of the fullerene derivative was prepared a day in advance with a concentration of 4 mg mL^{-1}. The solution was stirred on a hotplate at 45 °C for 5 hours and 15 minutes before spin-coating. For larger glass substrates measuring 2 × 2 cm^2, 150 µL of the solution was sufficient to cover the entire surface, while 80 µL was used for 2 × 1 cm^2 glass substrates. Spin-coating was performed in a single step by applying 3000 rpm for 30 seconds for each sample. Following spin-coating, the samples were dried on a hotplate at 45 °C for 1 minute and were ready for further investigation.

EI spectroscopy

The impedance was measured by applying an AC potential with a DC offset to the electrochemical cell, with the material of interest acting as the working electrode, and the current flowing through the cell was then measured. The obtained results were subsequently fitted with equivalent circuits containing different electrical elements, which represented the materials and interfaces of the inspected electrochemical cell. For the EIS measurements, an electrochemical cell was assembled using a water solution containing 5×10^{-4} mol dm^{-3} of $K_3[Fe(CN)_6]$, 5×10^{-4} mol dm^{-3} of $K_4[Fe(CN)_6]$, and 0.1 mol dm^{-3} of KCl as the electrolyte. The counter electrode was platinum mash. The measurements were conducted using the Ivium Vertex potentiostat with an impedance analyzer, and the IviumSoft software was used for fitting the obtained curves. The measurements were performed with an open circuit DC offset of 0.22 V and a 50 mA AC component. The frequency range was set to 0.1–10 000 Hz. The system was purged with nitrogen for 15 minutes before each measurement, and an equilibrium time of 60 s was set. All EIS fitting procedures were performed with a chi factor of 10^{-3}.

Cyclic voltammetry (CV) of the synthesized fullerene derivatives dissolved in solution was conducted at room temperature. Tetrabutylammonium hexafluorophosphate (nBu$_4$NPF$_6$) at a concentration of 0.1 M was used as a supporting electrolyte. The solvent employed was *o*-dichlorobenzene/dimethylformamide (*o*-DCB/DMF, 100 : 1 v/v). The reference electrode used was Ag/AgCl, and the working electrode was a glassy carbon electrode (GCE). The scan rate was set at 50 mV s^{-1}.

The investigation of the thin film of our compounds on **FTO** also employed CV experiments. The electrolyte used for this type of CV consisted of a water solution containing 5×10^{-4} mol dm^{-3} of $K_3[Fe(CN)_6]$, 5×10^{-4} mol dm^{-3} of $K_4[Fe(CN)_6]$, and 0.1 mol dm^{-3} of KCl. The voltammetric sweep ranged from −1 to 1 V. In this experiment, the samples as thin films on the **FTO** were connected as the working electrode, the platinum mash was used as the counter electrode, and the reference electrode was Ag/AgCl. All measurements were performed after a previous purging with N_2 for 10 minutes.

UV-Vis measurements of the fullerene derivatives, which had been deposited on the microscopic glasses, were analyzed in the wavelength range of 325–1000 nm.

Conflicts of interest

There are no conflicts to declare.

Acknowledgements

This research is funded by the Serbian Ministry of Science, Technological Development and Innovation, grant no. 451-03-47/2023-01/200026 and grant no. 451-03-9/2021-14/200168.

References

1 Y.-H. Kim, S. Kim, A. Kakekhani, J. Park, J. Park, Y.-H. Lee, H. Xu, S. Nagane, R. B. Wexler, D.-H. Kim, S. H. Jo, L. Martínez-Sarti, P. Tan, A. Sadhanala, G.-S. Park, Y.-W. Kim, B. Hu, H. J. Bolink, S. Yoo, R. H. Friend, A. M. Rappe and T.-W. Lee, *Nat. Photonics*, 2021, **15**, 148–155.
2 L. K. Ono, S. Liu and Y. Qi, *Angew. Chem., Int. Ed.*, 2020, **59**, 6676–6698.
3 Y. Zhou, J. Chen, O. M. Bakr and O. F. Mohammed, *ACS Energy Lett.*, 2021, **6**, 739–768.
4 L. Lei, Q. Dong, K. Gundogdu and F. So, *Adv. Funct. Mater.*, 2021, **31**, 2010144.
5 J. Jeong, M. Kim, J. Seo, H. Lu, P. Ahlawat, A. Mishra, Y. Yang, M. A. Hope, F. T. Eickemeyer, M. Kim, Y. J. Yoon, I. W. Choi, B. P. Darwich, S. J. Choi, Y. Jo, J. H. Lee, B. Walker, S. M. Zakeeruddin, L. Emsley, U. Rothlisberger, A. Hagfeldt, D. S. Kim, M. Grätzel and J. Y. Kim, *Nature*, 2021, **592**, 381–385.
6 M. A. Green, E. D. Dunlop, D. H. Levi, J. Hohl-Ebinger, M. Yoshita and A. W. Y. Ho-Baillie, *Prog. Photovoltaics Res. Appl.*, 2019, **27**, 565–575.
7 J. Benick, A. Richter, R. Müller, H. Hauser, F. Feldmann, P. Krenckel, S. Riepe, F. Schindler, M. C. Schubert, M. Hermle, A. W. Bett and S. W. Glunz, *IEEE J. Photovolt.*, 2017, **7**, 1171–1175.
8 J. Miao and F. Zhang, *J. Mater. Chem. C*, 2019, **7**, 1741–1791.
9 M. Nakamura, K. Yamaguchi, Y. Kimoto, Y. Yasaki, T. Kato and H. Sugimoto, *IEEE J. Photovolt.*, 2019, **9**, 1863–1867.
10 G. Nazir, S.-Y. Lee, J.-H. Lee, A. Rehman, J.-K. Lee, S. I. Seok and S.-J. Park, *Adv. Mater.*, 2022, **34**, 2204380.
11 Y. Wu, Q. Wang, Y. Chen, W. Qiu and Q. Peng, *Energy Environ. Sci.*, 2022, **15**, 4700–4709.
12 National Renewable Energy Laboratory Best Research-Cell Efficiencies, **https://www.nrel.gov/pv/assets/pdfs/best-research-cell-efficiencies.20191106.pdf**, NREL, 2019.
13 D. Bi, W. Tress, M. I. Dar, P. Gao, J. Luo, C. Renevier, K. Schenk, A. Abate, F. Giordano, J.-P. Correa Baena, J.-D. Decoppet, S. M. Zakeeruddin, M. K. Nazeeruddin, M. Grätzel and A. Hagfeldt, *Sci. Adv.*, 2016, **2**, e1501170.
14 T. Xue, D. Chen, T. Li, X. Chou, X. Wang, Z. Tang, F. Zhang, J. Huang, K. Guo and A. V. Takaloo, *Micromachines*, 2023, **14**, DOI: **10.3390/mi14061095**.
15 K. Wojciechowski, T. Leijtens, S. Siprova, C. Schlueter, M. T. Hörantner, J. T.-W. Wang, C.-Z. Li, A. K. Y. Jen, T.-L. Lee and H. J. Snaith, *J. Phys. Chem. Lett.*, 2015, **6**, 2399–2405.
16 M. Prato, *J. Mater. Chem.*, 1997, **7**, 1097–1109.
17 J. C. Hummelen, B. W. Knight, F. LePeq, F. Wudl, J. Yao and C. L. Wilkins, *J. Org. Chem.*, 1995, **60**, 532–538.
18 D. Chi, S. Qu, Z. Wang and J. Wang, *J. Mater. Chem. C*, 2014, **2**, 4383–4387.
19 Z. Sun, M. Liu, Y. Zhou, Q. Wang, Y. Yang, Y. Zhou and F. Liu, *Sol. Energy Mater. Sol. Cells*, 2022, **235**, 111453.
20 D. Payno, Y. Sánchez, O. Blázquez, S. Giraldo, M. Salado, S. Kazim, E. Saucedo and S. Ahmad, *J. Mater. Chem. C*, 2020, **8**, 12533–12542.

21 Y. Wang, L. Wang, Y. Wang, X. Zhao, X. Zhang, X. Zhang and Y. Liu, *Phys. Status Solidi RRL*, 2023, 2300186.
22 G. Tchutchulashvili, K. P. Korona, W. Mech, S. Chusnutdinow, M. Sobanska, K. Klosek, Z. R. Zytkiewicz and W. Sadowski, *J. Nanopart. Res.*, 2020, **22**, 1–9.
23 M. Ai, M. Chen and S. Yang, *Chin. J. Chem.*, 2023, **41**, 2337–2353.
24 S. Liu, V. P. Biju, Y. Qi, W. Chen and Z. Liu, *NPG Asia Mater.*, 2023, **15**, 27.
25 Y. Zhong, M. Hufnagel, M. Thelakkat, C. Li and S. Huettner, *Adv. Funct. Mater.*, 2020, **30**, 1908920.
26 R. Zahran and Z. Hawash, *Adv. Mater. Interfaces*, 2022, **9**, 2201438.
27 A. A. Said, J. Xie and Q. Zhang, *Small*, 2019, **15**, 1900854.
28 A. B. Sieval, N. D. Treat, D. Rozema, J. C. Hummelen and N. Stingelin, *Chem. Commun.*, 2015, **51**, 8126–8129.
29 S. Erten-Ela, H. Chen, A. Kratzer, A. Hirsch and C. J. Brabec, *New J. Chem.*, 2016, **40**, 2829–2834.
30 Y. Xing, C. Sun, H. L. Yip, G. C. Bazan, F. Huang and Y. Cao, *Nano Energy*, 2016, **26**, 7–15.
31 S. Shao, M. Abdu-Aguye, L. Qiu, L.-H. Lai, J. Liu, S. Adjokatse, F. Jahani, M. E. Kamminga, G. H. ten Brink, T. T. M. Palstra, B. J. Kooi, J. C. Hummelen and M. A. Loi, *Energy Environ. Sci.*, 2016, **9**, 2444–2452.
32 Y. Bai, Q. Dong, Y. Shao, Y. Deng, Q. Wang, L. Shen, D. Wang, W. Wei and J. Huang, *Nat. Commun.*, 2016, **7**, 12806.
33 M. M. Elnaggar, A. V. Mumyatov, N. A. Emelianov, L. G. Gutsev, V. V. Ozerova, I. V. Fedyanin, Y. V. Nelyubina, S. I. Troyanov, B. R. Ramachandran and P. A. Troshin, *Sustainable Energy Fuels*, 2023, **7**, 3893–3901.
34 J. Jakšić, A. Mitrović, Z. Tokić Vujošević, M. Milčić and V. Maslak, *RSC Adv.*, 2021, **11**, 29426–29432.
35 J. Jakšić, I. Solymosi, A. Hirsch, M. E. Pérez-Ojeda, A. Mitrović and V. Maslak, *Chem. – Eur. J.*, 2023, **29**, e202301061.
36 C. I. Wang and C. C. Hua, *J. Phys. Chem. B*, 2015, **119**, 14496–14504.
37 K. Kutlu, P. Kavak, E. A. Parlak, A. E. Saatci, F. P. Gökdemir, U. D. Menda and O. Özdemir, *AIP Conf. Proc.*, 2013, **1569**, 283–287.
38 T. E. Saraswati, U. H. Setiawan, M. R. Ihsan, I. Isnaeni and Y. Herbani, *Open Chem.*, 2019, **17**, 1198–1212.
39 I. Gutiérrez-González, B. Molina-Brito, A. W. Götz, F. L. Castillo-Alvarado and J. I. Rodríguez, *Chem. Phys. Lett.*, 2014, **612**, 234–239.
40 P. Topolovsek, F. Lamberti, T. Gatti, A. Cito, J. M. Ball, E. Menna, C. Gadermaier and A. Petrozza, *J. Mater. Chem. A*, 2017, **5**, 11882–11893.
41 M. H. Elbakkay, W. M. A. El Rouby, A. Mariño-López, A. Sousa-Castillo, V. Salgueiriño, S. I. El-Dek, A. A. Farghali, M. A. Correa-Duarte and P. Millet, *Int. J. Hydrogen Energy*, 2021, **46**, 31216–31227.
42 Z. Liu, J. Siekmann, B. Klingebiel, U. Rau and T. Kirchartz, *Adv. Energy Mater.*, 2021, **11**, 2003386.